arXiv:1612.05188v1 [math.AP] 15 Dec 2016

Investigation of a Structured Fisher's Equation with Applications in Biochemistry

John T. Nardini*, D.M. Bortz*

December 16, 2016

Abstract

Recent biological research has sought to understand how biochemical signaling pathways, such as the mitogen-activated protein kinase (MAPK) family, influence the migration of a population of cells during wound healing. Fisher's Equation has been used extensively to model experimental wound healing assays due to its simple nature and known traveling wave solutions. This partial differential equation with independent variables of time and space cannot account for the effects of biochemical activity on wound healing, however. To this end, we derive a structured Fisher's Equation with independent variables of time, space, and biochemical pathway activity level and prove the existence of a self-similar traveling wave solution to this equation. We also consider a more complicated model with different phenotypes based on MAPK activation and numerically investigate how various temporal patterns of biochemical activity can lead to increased and decreased rates of population migration.

keywords: Stage-structure, Traveling Wave Solutions, Wound Healing, Biochemical Signaling Pathways

1 Introduction

Traveling wave solutions to partial differential equations (PDEs) are often used to study the collective migration of a population of cells during wound healing [5, 11, 26, 27, 29], tumorigenesis [25], and angiogenesis [40, 43]. R.A. Fisher introduced what is now referred to as Fisher's Equation in 1937 to model the advance of an advantageous gene in a population [14]. Since then, it has been used extensively in math biology literature to model the migration of a monolayer of cells during experimental wound healing assays [5, 20, 29].

Fisher's Equation is written as

$$u_t = Du_{xx} + \lambda u(K - u) \tag{1}$$

*Department of Applied Mathematics, University of Colorado, Boulder 80309-0526, United States (john.nardini@colorado.edu, dmbortz@colorado.edu)

with subscripts denoting differentiation with respect to that variable and $u = u(t,x)$ representing a population of cells over time t at spatial location x. The first term on the right hand side of (1) represents diffusion in space with rate of diffusion, D, and the second term represents logistic growth of the population with proliferation rate, λ, and carrying capacity, K. As shown in [35, § 11.2], (1) admits traveling wave solutions of the form

$$u(t,x) = U(z),\ z = x - ct$$

where c denotes the speed of the traveling wave solution and $U(z)$ denotes the traveling wave profile. Traveling wave solutions to (1) thus maintain a constant profile, $U(z)$, over time that moves leftward if $c < 0$ or rightward if $c > 0$ with speed $|c|$. It is also shown that (1) has a positive and monotonic profile for $|c| \geq 2\sqrt{D\lambda}$, which is biologically relevant when $u(t,x)$ denotes a population of cells. Kolmogoroff proved in 1937 that any solution to (1) with a compactly-supported initial condition will converge to a traveling wave solution with minimum wavespeed $c = 2\sqrt{D\lambda}$ [24]. See [34, § 5.4] for a proof of this. There is also a wide literature on studies into extensions of Fisher's Equation, such as Fisher's Equation coupled with chemotaxis [2, 26], time-dependent rates of proliferation and diffusion [18], and space-dependent rates of diffusion [9].

Structured population models, or PDE models with independent variables to distinguish individuals by some continuously-varying properties, were first investigated via age-structured models in the early 20th century [32, 42]. The 1970s saw a revival in structured population modeling after the introduction of methods to investigate nonlinear structured population models [17], which led to our current understanding of semigroup theory for linear and nonlinear operators on Banach spaces [50]. Several recent biological studies have demonstrated the existence of traveling wave solutions to structured population models [12, 13, 15, 45], and another study used an independent variable representing subcellular β-catenin concentration to investigate how signaling mutations can cause intestinal crypts to invade healthy neighboring crypts [36].

Recent biological research has focused on the influence of biochemical signaling pathways on the migration of a population of cells during wound healing. Particular emphasis has been placed on the mitogen-activated protein kinase (MAPK) signaling cascade, which elicits interesting patterns of activation and migration in response to different types of cytokines and growth factors in various cell lines [7, 31]. For example, experimental wounding assays of madine darby canine kidney cells (MDCKs) in [31] yielded a transient pulse of ERK 1/2 (a specific MAPK protein) activity in the cell sheet that only lasted for a few minutes. This pulse of activity was followed by a slow wave of activity that propagated from the wound margin to submarginal cells over the course of several hours. The second wave was determined to be crucial for regulating MDCK sheet migration. The authors of [31] proposed that these fast and slow waves of ERK 1/2 activity could be caused by the production of reactive oxygen species (ROS) and epidermal growth factor (EGF), respectively. Similar experiments with fibroblasts also demonstrated this first transient wave of ERK 1/2

activity, but not the following slow wave. The authors of [7] found that human keratinocyte (HaCaT) cells exhibit ERK 1/2 activity primarily at the wound margin during similar experimental wound healing assays with a high density in response to treatment with transforming growth factor-β (TGF-β).

In this study, we detail an approach to investigate a structured version of Fisher's Equation that is motivated by the above experimental observations. Previous structured population models have been restricted to traits that primarily increase over time, such as age or size, but our analysis allows for both activation and deactivation along the biochemical activity dimension.

In Section 2, we develop our structured population model and devote Section 3 to a review of relevant material from size-structured population models. We demonstrate the existence of self-similar traveling wave solutions to the model in Section 4. We then study a more complicated version of our model where migration and proliferation of the population depend on MAPK activity levels in Section 5 before making final conclusions and discussing future work in Section 6.

2 Model Development

We model a cell population during migration into a wound, denoted by $u(t, x, m)$, for

$$u : [0, \infty) \times \mathbb{R} \times [m_0, m_1] \to \mathbb{R}$$

where t denotes time, x denotes spatial location, and m denotes activation along a biochemical signaling pathway with minimum and maximum levels m_0 and m_1, respectively. As a first pass, we assume that any cells of the same MAPK activity level will activate identically over time in the same environment. This assumption allows us to model the activation distribution of the population over time deterministically by considering how cells of all possible MAPK activity levels activate and deactivate over time. We note that biochemical signaling is an inherently heterogeneous process, so our approach would benefit from a further investigation with stochastic differential equations.

As discussed in [10], crucial aspects of a structured population model include the individual state, the environmental state, external forcing factors, and feedback functions. The *individual state* is a dimension used to distinguish between individuals of a population and is typically based on physiological properties such as age or size. As activation of biochemical signaling pathways influences cell migration through diffusive and proliferative properties of cells, we incorporate the biochemical activity dimension, m, as an individual state for our model.

The *environmental state* of a population is the external factors that influence individual behavior. Recall that external cytokines and growth factors, such as ROS, TGF-β, and EGF, influence activation of the MAPK signaling cascade and promote migration during wound healing. The cell population will not directly affect the level of external growth factor in this work, so an *external forcing factor* will be used to represent treatment with these chemicals here.

The external chemical concentration at time t will be denoted by $s(t)$, and the activation response of cells to this chemical will be given by the function $f(s)$.

A *feedback function* included in our work will be the inhibition of individual cell proliferation in response to a confluent density. As proliferation is hindered by contact inhibition, we introduce a new variable,

$$w(t,x) := \int_{m_0}^{m_1} u(t,x,m)dm \tag{2}$$

to represent the population of cells at time t and spatial location x. Proliferation of the population will accordingly vanish as $w(t,x)$ approaches the carrying capacity, K.

Our model, which we term as a *structured Fisher's Equation*, is given by the PDE:

$$\begin{aligned} u_t + \underbrace{(f(s(t))g(m)u)_m}_{activation} &= \underbrace{D(m)u_{xx}}_{diffusion} + \underbrace{\lambda(m)u\left(K - w(t,x)\right)}_{population\ growth} \\ w(t,x) &= \int_{m_0}^{m_1} u(t,x,m)dm \\ u(t=0,x,m) &= \phi(x,m) \\ u(t,x,m=m_1) &= 0 \\ w(t,-\infty) = K \qquad & \qquad w(t,x=+\infty) = 0 \end{aligned} \tag{3}$$

The function $g(m) \in C^1([m_0, m_1])$ denotes the rate of biochemical activation in the population, $s(t) \in L^\infty(\mathbb{R}^+)$ denotes the external chemical concentration in the population, $f(s) \in L^1_{loc}(0,\infty)$ denotes the activation response of cells to the level of signaling factor present, $D(m)$ and $\lambda(m)$ denote biochemically-dependent rates of cell diffusion and proliferation, and $\phi(x,m)$ denotes the initial condition of u. The spatial boundary conditions specify that the cell density has a confluent density at $x = -\infty$ and an empty wound space at $x = +\infty$. We use a no flux boundary condition at $m = m_1$ so that cells cannot pass this boundary. In the remainder of this study, we will write $f(s(t))$ as $f(t)$ for simplicity, though we note that this function will differ between cell lines that respond differently to the same chemical during wound healing[1].

The solution space of (3), $\mathcal{D}$, is defined with inspiration from [50] and [49, § 1.1]. If we let Z denote the space of bounded and twice continuously differentiable functions on $\mathbb{R}$, then we define

$$\mathcal{D} := \left\{ u(t,x,m) \,\middle|\, \int_{m_0}^{m_1} u(t,x,m)dm \in Z \right\},$$

i.e., $u(t,x,m) \in \mathcal{D}$ if $w(t,x) \in Z$ for all $t > 0$. We note that $\int_{m_0}^{m_1} \phi(x,m)dm$ need only be bounded and piecewise continuous with a finite number of discontinuities

[1] Note that an extension for modeling the dynamics governing $s(t)$ will be considered in a future study.

[49]. If $\phi(x,m)$ is not sufficiently smooth in m, we obtain generalized solutions of (3) [50].

In Section 4, we will investigate (3) with constant rates of diffusion and proliferation (i.e., $D(m) = D, \lambda(m) = \lambda$) and $f(t) = 1$. By substituting

$$\begin{aligned} u^* = u/K, \qquad & t^* = \lambda K t, \\ x^* = x\sqrt{\lambda K/D}, \qquad & m^* = (m - m_0)/(m_1 - m_0), \\ g^*(m^*) = \qquad & g(m^*(m_1 - m_0) + m_0)/(\lambda K m_1), \end{aligned}$$

and dropping asterisks for simplicity, (3) can be non-dimensionalized to

$$\begin{aligned} u_t + \underbrace{(f(t)g(m)u)_m}_{activation} &= \underbrace{u_{xx}}_{diffusion} + \underbrace{u\left(1 - \int_0^1 u(t,x,m)dm\right)}_{population\ growth} \qquad (4) \\ w(t,x) &= \int_0^1 u(t,x,m)dm \\ u(t=0,x,m) &= \phi(x,m) \\ u(t,x,m=1) &= 0 \\ w(t,x=-\infty) = 1 \qquad & w(t,x=+\infty) = 0. \end{aligned}$$

In Section 5, we will consider the full model (3) when the rates of cellular diffusion and proliferation are piece-wise constant functions of m and numerically investigate how different functions for $f(t)$ lead to increased and decreased levels of population migration.

3 Background Material from Size-Structured Population Modeling

Before investigating the existence of traveling-wave solutions to (4), it is useful to review some key topics used to solve size-structured population models, as discussed in [50]. These topics will be useful in analyzing (3) in later sections. A reader familiar with using the method of characteristics to solve size-structured population models may briefly skim over this section to pick up on the notation used throughout our study.

As an example, we consider the size-structured model given by

$$\begin{aligned} u_t + (g(y)u)_y &= Au \qquad (5) \\ u(t=0,y) &= \phi(y) \end{aligned}$$

where $u = u(t,y) : [0,\infty) \times [y_0, y_1] \to \mathbb{R}$ denotes the size distribution over y of a population at time t, y_0 and y_1 denote the minimum and maximum population sizes respectively, and $g(y) \in C^1(([y, y_1])$ denotes the physical growth rate[2]

[2]Note that in this section, $g(y)$ denotes a growth rate with respect to size, y, whereas throughout the rest of our study, $g(m)$ denotes an activation rate with respect to biochemical activity, m.

of individuals of size y. In this section, we will work in the Banach space $\mathbb{X} = L^1((y_0, y_1) \to \mathbb{R})$, and assume $A \in \mathcal{B}(\mathbb{X})$, the space of bounded, linear operators on $\mathbb{X}$. The method of characteristics will facilitate solving (5).

For a fixed size $\underline{y} \in [y_0, y_1]$, the function

$$\sigma(y; \underline{y}) := \int_{\underline{y}}^{y} \frac{1}{g(y')} dy' \tag{6}$$

provides *the time it takes for an individual to grow from the fixed size $\underline{y}$ to arbitrary size y*. If $g(y)$ is positive and uniformly continuous on $[y_0, y_1]$, then $\sigma(y; \underline{y})$ is invertible. We denote the inverse function, $\sigma^{-1}(t; \underline{y})$, as the *growth curve*, and it computes *the size of an individual over time that starts at size $\underline{y}$ at time $t = 0$*. For instance, if an individual has size $\underline{y}$ at $t = 0$, then that individual will have size $\sigma^{-1}(t_1; \underline{y})$ at time $t = t_1$. Some helpful properties of the growth curve are that $\sigma^{-1}(0; \underline{y}) = \underline{y}$ and

$$\frac{d}{dt}\sigma^{-1}(t; \underline{y}) = g(\sigma^{-1}(t; \underline{y})). \tag{7}$$

See Section A in the appendix for the derivation of (7).

In order to solve (5) with the method of characteristics, we set $y = \sigma^{-1}(t; \underline{y})$ to define the variable $v(t; \underline{y})$:

$$v(t; \underline{y}) := u(t, y = \sigma^{-1}(t; \underline{y})). \tag{8}$$

As shown in Section B of the appendix, substitution of (8) into (5) yields the characteristic equation

$$v_t = -g'(\sigma^{-1}(t; \underline{y}))v + Av, \tag{9}$$

where primes denote differentiation with respect to y. This characteristic equation has size $\underline{y}$ at time $t = 0$ and can be solved explicitly as[3]

$$v(t; \underline{y}) = \frac{g(\underline{y})}{g(\sigma^{-1}(t; \underline{y}))} e^{At} \phi(\underline{y}). \tag{10}$$

As (10) provides the solution to (5) along the arbitrary characteristic curve with initial size $\underline{y}$, we use it to solve the whole equation with the substitution $y = \sigma^{-1}(t, \underline{y})$, in which we find

$$u(t, y) = \begin{cases} \frac{g(\sigma^{-1}(-t, y))}{g(y)} e^{At} \phi(\sigma^{-1}(-t, y)) & \sigma^{-1}(t; y_0) \le y \le y_1 \\ 0 & y_0 \le y < \sigma^{-1}(t; y_0). \end{cases} \tag{11}$$

If $\phi(y) \notin C^1(y_0, y_1)$, then (11) is viewed as a generalized solution. Note that a piecewise form is needed for (11) because we do not have any individuals below

[3]To derive this, use separation of variables and with the help of (7) note that $\int_0^t g'(\sigma^{-1}(\tau; \underline{y}))d\tau = \ln[g(\sigma^{-1}(t; \underline{y}))/g(\underline{y})]$.

the minimum size, y_0, and thus the minimum possible size at time t is given by $\sigma^{-1}(t; y_0)$. If the population is assumed to give birth to individuals of size y_0 over time, then the appropriate renewal equation representing population birth would replace the zero term in the piecewise function (see [3, § 9.5] for an example in size-structured populations and [15] for an example in age-structured populations).

4 Existence of Traveling Wave Solutions to the Structured Fisher's Equation

4.1 Existence of traveling wave solutions to (4)

We now incorporate topics from the previous section to show the existence of traveling wave solutions to (4). After taking the time derivative of $w(t, x)$, which was defined in (2), we can rewrite (4) as a system of two coupled PDEs[4]:

$$\begin{aligned} u_t + (g(m)u)_m &= u_{xx} + u(1 - w) \\ w_t &= w_{xx} + w(1 - w). \end{aligned} \tag{12}$$

Note that in this section, $g(m)$ is a function of biochemical activity level and $\sigma^{-1}(t; \underline{m})$ computes *the activity level of an individual over time that starts at level* $\underline{m}$ *at time* $t = 0$. We will thus now refer to $\sigma^{-1}(t; \underline{m})$ as the *activation curve*. We next set up the characteristic equation for u by setting $m = \sigma^{-1}(t; \underline{m})$ for a fixed value of $\underline{m}$:

$$v(t, x; \underline{m}) := u(t, x, m = \sigma^{-1}(t; \underline{m})). \tag{13}$$

Substituting (13) into (12) simplifies to our characteristic equation

$$\begin{aligned} v_t &= v_{xx} + v[1 - w - g'(\sigma^{-1}(t; \underline{m}))] \\ w_t &= w_{xx} + w(1 - w), \end{aligned} \tag{14}$$

a nonautonomous system of two coupled PDEs in time and space. Note that the bottom equation for (14) is Fisher's Equation, which has positive monotonic traveling wave solutions for any speed $c \geq 2$ (see [35, § 11.2]).

We next aim to derive traveling wave solutions to (14), however, we are not aware of any traveling wave solutions to nonautonomous systems such as this one. From our knowledge of size-structured population models from Section 3, we instead intuit the ansatz of a self-similar traveling wave solution, which we write as

$$\begin{aligned} v(t, x; \underline{m}) &= \frac{g(\underline{m})}{g(\sigma^{-1}(t; \underline{m}))} V(z), \ z = x - ct \\ w(t, x) &= W(z). \end{aligned} \tag{15}$$

[4]Note that either $g(m_0) = 0$ or $u(t, m = m_0, x) = 0$ for $t > 0$, so that the activation term drops out when integrating over m for w.

In this ansatz, $V(z)$ will define a traveling wave profile for v and $\frac{g(\underline{m})}{g(\sigma^{-1}(t;\underline{m}))}$ will provide the height of the function over time. With the aid of the chain rule, we observe that:

$$\begin{aligned} v_t(t,x;\underline{m}) &= \frac{g'(\sigma^{-1}(t;\underline{m}))g(\sigma^{-1}(t;\underline{m}))}{g(\underline{m})}V - c\frac{g(\sigma^{-1}(t;\underline{m}))}{g(\underline{m})}V_z \\ v_{xx}(t,x;\underline{m}) &= \frac{g(\sigma^{-1}(t;\underline{m}))}{g(\underline{m})}V_{zz}, \end{aligned}$$

where subscripts denote differentiation with respect to t, x, or z and primes denote differentiation with respect to m. Substituting (15) into (14) reduces to the autonomous system

$$\begin{aligned} -cV_z &= V_{zz} + V(1-W) \\ -cW_z &= W_{zz} + W(1-W). \end{aligned} \tag{16}$$

It is now useful to rewrite (16) as the first order system

$$\frac{d}{dz}\boldsymbol{\mathcal{V}} = \begin{pmatrix} V_z \\ -cV_z - V(1-W) \\ W_z \\ -cW_z - W(1-W) \end{pmatrix} \tag{17}$$

for $\boldsymbol{\mathcal{V}}(z) = [V(z), V_z(z), W(z), W_z(z)]^T$. Recall that profiles to traveling wave solutions can be constructed with heteroclinic orbits between equilibria for a given dynamical system (or homoclinic orbits for a traveling pulse) [22, § 6.2]. We observe two types of equilibria for (16), given by $\boldsymbol{\mathcal{V}}_1^* = (1,0,V,0)^T$ and $\boldsymbol{\mathcal{V}}_2^* = \vec{0}$, where the former represents a confluent cell density and the latter represents an empty wound space. We accordingly search for heteroclinic orbits from $\boldsymbol{\mathcal{V}}_1^*$ to $\boldsymbol{\mathcal{V}}_2^*$ for some $c > 0$. We choose to focus on the characteristic equations $v(t,x,m = \sigma^{-1}(t;\underline{m}))$ for values of $\underline{m}$ in which $\phi(\underline{m}, x = -\infty) > 0$ to represent the population of cells migrating into the empty wound space. We thus denote $\boldsymbol{\mathcal{V}}_1^* = (1,0,\nu,0)^T$ for $\nu > 0$.

Note that $\boldsymbol{\mathcal{V}}_1^*$ is an equilibrium for any value of V, as $W = 1$ will guarantee the existence of an equilibrium. Such a "continuum" of equilibria was also observed in [39]. This structure of $\boldsymbol{\mathcal{V}}_1^*$ yields a zero eigenvalue after linearizing (17) about $\boldsymbol{\mathcal{V}}_1^*$, so we cannot use linear theory to study the local behavior of (17) near $\boldsymbol{\mathcal{V}}_1^*$. While we could construct the unstable manifold of (17) using a power series representation to study its local behavior around $\boldsymbol{\mathcal{V}}_1^*$ (see [33, Section 5.6]), we find it more insightful to define a trapping region in the (V, V_z)-plane as has been done in previous traveling wave studies [2, 25]. We will then use asymptotically autonomous phase-plane theory to describe the ω-limit set of our flow, which will show the existence of a heteroclinic orbit from $\boldsymbol{\mathcal{V}}_1^*$ to $\boldsymbol{\mathcal{V}}_2^*$. *Trapping regions* are positively invariant regions with respect to the flow of a dynamical system, and the *ω-limit set* of a flow is the collection all limit point of that flow [33, § 4.9-10].

We study the trajectory of $\boldsymbol{\mathcal{V}}$ in the (V, V_z)-plane by defining the triangular region bound by the lines $\{V = \nu, V_z = 0, V_z = -\frac{c}{2}V\}$ and denoting this region as Δ. The following lemma will demonstrate that Δ is a trapping region for the flow of (17) in the (V, V_z)-plane.

Lemma: Let $\nu > 0$ and $c \geq 2$. Then the region Δ is positively invariant with respect to (17) so long as $0 < W(z) < 1$ for all $z \in \mathbb{R}$.

Proof:

We prove this lemma by investigating the vector field along each of the lines specifying the boundary of our region and showing that they point into the interior of the space.

i.) Along the line $V_z = 0$, $\frac{d}{dz}V_z = -V(1-W)$, which is nonpositive because $W(z) < 1$ for all $z \in \mathbb{R}$ and our region is defined for $V(z) \geq 0$. If $V = 0$,then we are at the equilibrium point $(V, V_z) = (0, 0)$.

ii.) Along $V = \nu$, $\frac{d}{dz}V = V_z$, which is negative in our defined region. The only point to worry about here is at $(V, V_z) = (\nu, 0)$, as then $\frac{d}{dz}V = 0$. However, we see from part i.) that $\frac{d}{dz}V_z < 0$ here, so that a flow starting at $(\nu, 0)$ will initially move perpendicular to the V-axis in the negative V_z direction, and then $\frac{d}{dz}V < 0$, so the flow enters Δ.

iii.) Note that the inner normal vector to the line $V_z = -\frac{c}{2}V$ is $\hat{n} = \left(\frac{c}{2}, 1\right)$. Then

$$\begin{aligned}
\hat{n} \cdot \frac{d}{dz}(V, V_z) &= \left(\frac{c}{2}, 1\right) \cdot (V_z, -cV_z - V + VW) \\
&= \left(\frac{c}{2}, 1\right) \cdot (-\frac{c}{2}V, \frac{c^2}{2}V - V + VW) \\
&= -\frac{c^2}{4}V + \frac{c^2}{2}V - V + VW \\
&= V\left(\frac{c^2}{4} - 1\right) + VW,
\end{aligned}$$

which is positive, as $c \geq 2$.□

This proof is visually demonstrated in the top row of Figure 1. As $W(z)$ has a heteroclinic orbit with $W(-\infty) = 1$ and $W(\infty) = 0$ for any $c \geq 2$ [35, § 11.2], we conclude that Δ is a positively invariant set for the flow of (17) in the (V, V_z). The following corollary describes the ω-limit set of (17).

Corollary: The ω-limit set of (17) starting at $\boldsymbol{\mathcal{V}}_2^*$, $\omega(\boldsymbol{\mathcal{V}}_2^*)$, is $\boldsymbol{\mathcal{V}}_1^*$.

Proof:

As $W(z) \to 0$ as $z \to +\infty$, then the vector field for (17) in the (V, V_z)-plane is asymptotically autonomous to the vector field

$$\frac{d}{dz}\begin{pmatrix} V \\ V_z \end{pmatrix} = \begin{pmatrix} V_z \\ -cV_z - V \end{pmatrix}, \tag{18}$$

a linear system whose only equilibrium is the origin. As $c \geq 2$, the origin is a stable equilibrium and the flow of the limiting system remains in Δ, and hence the fourth quadrant, for all time.

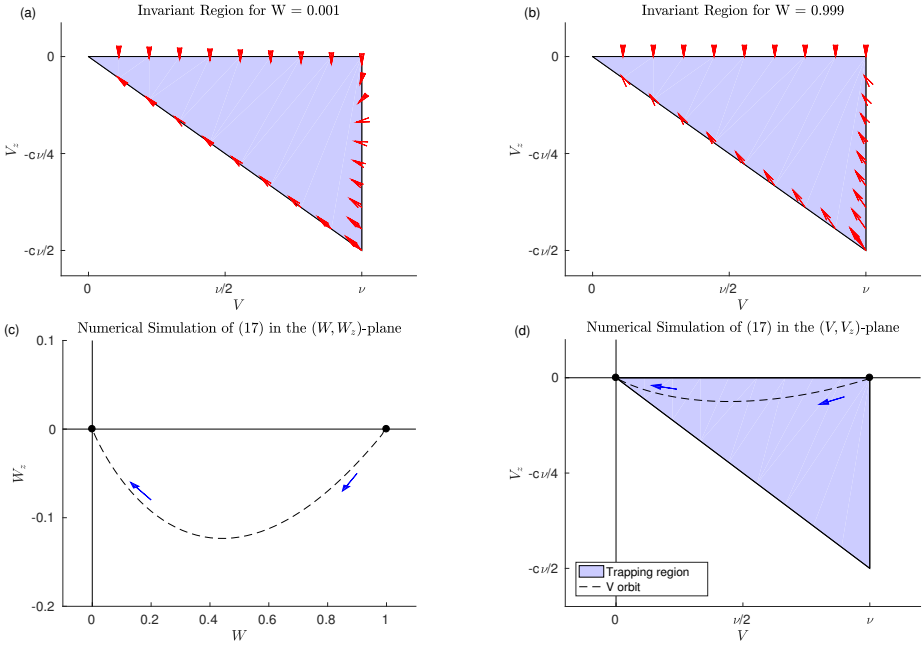

Figure 1: Construction of the heteroclinic orbit between $\boldsymbol{\mathcal{V}}_1^*$ and $\boldsymbol{\mathcal{V}}_2^*$ for (17). In (a) and (b), we depict the trapping region in the (V, V_z)-plane, Δ, and the vector field along its boundary for $\alpha = 0.5, c = 2.3, W_z = 0$ and W near 0 and 1, respectively. In (c) and (d), we depict numerical simulations of (17) in the (W, W_z)-plane and in the (V, V_z)-plane, respectively. Arrows denote the direction of the flow and the black dots mark equilibria of (17).

As $^d/_{dz}V = V_z < 0$ in Δ, no periodic or homoclinic orbits can exist for the limiting system. We thus conclude from the asymptotically autonomous Poincare-Bendixson Theorem presented in [30][5] that our flow in the (V, V_z) plane starting at $(\nu, 0)$ will limit to the origin. We conclude that $\omega(\boldsymbol{\mathcal{V}}_2^*) = \boldsymbol{\mathcal{V}}_1^*$.□

4.2 Summary of results

We have demonstrated the existence of self-similar traveling wave solutions to (4) in this section of the form

$$u(t, x, m) \quad = \quad \frac{g(\underline{m})}{g(\sigma^{-1}(t; \underline{m}))} V(z; \underline{m}), \ z = x - ct$$

for $c \geq 2$ and values of $\underline{m}$ where the initial condition $\phi(x = -\infty, \underline{m}) > 0$ and $V(z; \underline{m}) = u(x - ct, m = \sigma^{-1}(t; \underline{m}))$. Setting $m = \sigma^{-1}(t, \underline{m})$, then this can be

[5]The relevant theorem statement is given in Appendix C. We note that while the results of [30] are sufficient for our study, asymptotically autonomous systems have been more extensively studied in [4, 6, 47, 48] and a more comprehensive result in describing the ω-limit set of the asymptotically autonomous flow is given in [48].

written more explicitly as

$$u(t,x,m) = \begin{cases} \frac{g(\sigma^{-1}(-t,m))}{g(m)} V(z;\sigma^{-1}(-t;m)), & \sigma^{-1}(t;0) \le m < 1 \\ 0 & \text{otherwise} \end{cases}$$

and

$$\int_0^1 u(t,x,m)dm = w(t,x) = W(z)$$

where $[V(z;\underline{m}), W(z)]^T$ satisfies (16). An example height function $\frac{g(\sigma^{-1}(-t,m))}{g(m)}$ for trajectories along the activation curves $m = \sigma^{-1}(t;\underline{m})$ will be demonstrated later in Figure 3.

5 Structured Fisher's Equation with MAPK-dependent Phenotype

We now study a version of Fisher's Equation where cellular migration and proliferation depend on biochemical activity, m. Various cell lines have reduced rates of proliferation and increased migration in response to MAPK activation [7, 8, 31], so we let m denote activity along the MAPK signaling cascade in this section. We consider a model with two subpopulations: one with a high rate of diffusion in response to MAPK activation and the other with a high rate of proliferation when MAPK levels are low. MAPK activation will depend on an external forcing factor to represent the presence of an extracellular signaling chemical, such as ROS, TGF-β, or EGF. While the method of characteristics is not applicable to spatial activation patterning here due to the parabolic nature of (3) in space, we can investigate temporal patterns of activation and deactivation. *We will exhibit simple scenarios that give rise to three ubiquitous patterns of biochemical activity: 1.) a sustained wave of activation, 2.) a single pulse of activitation, and 3.) periodic pulses of activation.*

Before describing these examples, we first introduce some tools to facilitate our study of (3). We will detail some assumptions that simplify our analysis in Section 5.1, solve and compute the population activation profile over time and use it to define some activation criteria in Section 5.2, and discuss numerical issues and the derivation of a nonautonomous averaged Fisher's Equation in Section 5.3 before illustrating the different activation patterns and their effects on migration in Section 5.4.

5.1 Model Description

Recall that the full structured Fisher's Equation is given by

$$
\begin{aligned}
u_t + (f(t)g(m)u)_m &= D(m)u_{xx} + \lambda(m)u\,(1-w) \qquad (19)\\
w &= \int_{m_0}^{m_1} u(t,x,m)dm\\
u(t=0,x,m) &= \phi_1(m)\phi_2(x)\\
u(t,x,m=m_1) &= 0\\
w(t,x=+\infty)=0 &\qquad w(t,x=-\infty)=1.
\end{aligned}
$$

We have chosen the separable initial condition $u(t=0,x,m)=\phi_1(m)\phi_2(x)$ for simplicity. Given some $m_{crit}\in(m_0,m_1)$, we define two subsets of $[m_0,m_1]$ as $M_{inact}:=[m_0,m_{crit}], M_{act}:=(m_{crit},m_1]$, and the rates of diffusion and proliferation by

$$
D(m):=\begin{cases} D_1 & m\in M_{inact}\\ D_2 & m\in M_{act}\end{cases},\ \lambda(m):=\begin{cases}\lambda_1 & m\in M_{inact}\\ \lambda_2 & m\in M_{act}\end{cases} \qquad (20)
$$

for $D_1<D_2$ and $\lambda_2<\lambda_1$. Hence for $m\in M_{inact}$, the population is termed as *inactive* and primarily proliferates whereas for $m\in M_{act}$, the population is termed as *active* and primarily diffuses.

We let $supp(\phi_1(m))=[\underline{m}_{\min},\underline{m}_{\max}]$ for $\underline{m}_{\max}<m_{crit}$ and assume that $\int_{m_0}^{m_1}\phi_1(m)dm=1$ so $\phi_1(m)$ represents a probability density function for the initial distribution of cells in m. We accordingly denote

$$
\Phi_1(m):=\begin{cases}0 & m\le m_0\\ \int_{m_0}^{m}\phi_1(m')dm' & m_0<m\le m_1\\ 1 & m_1<m\end{cases}
$$

as the cumulative distribution function for $\phi_1(m)$.

5.2 Activation Profile and Activation Criteria

An interesting question is how the distribution of (19) along m changes over time. To answer this question, we consider (19) in terms of t and m, which we will write as $p(t,m)$ and call the *activation profile*:

$$
\begin{aligned}
p_t + (f(t)g(m)p)_m &= 0 \qquad (21)\\
p(0,m) &= \phi_1(m).
\end{aligned}
$$

Following the analysis from Section 3, we can solve (21) analytically. We integrate (21) along the *activation curves*, $h(t;\underline{m})$, which now are given by

$$
m=h(t;\underline{m}):=\sigma^{-1}\left(F(t);\underline{m}\right), \qquad (22)
$$

where $F(t):=\int_0^t f(\tau)d\tau$ denotes a cumulative activation function. We find the activation profile to be:

$$
p(t,m)=\begin{cases}\frac{g(\sigma^{-1}(-F(t),m))}{g(m)}\phi_1(\sigma^{-1}(-F(t),m)) & h(t;m_0)\le m\le m_1\\ 0 & m_0\le m<h(t;m_0).\end{cases} \qquad (23)
$$

Now we can derive a condition for a cell population starting in the inactive population to enter the active population. We see from (23) that the population will enter the active population if

$$h(t; \underline{m}_{\max}) > m_{crit} \iff F(t) > \sigma(m_{crit}; \underline{m}_{\max}) \tag{24}$$

for some values of t. By standard calculus arguments, (24) will occur if

$$F(t_{\max}) > \sigma(m_{crit}; \underline{m}_{\max}) \tag{25}$$

where a local maximum for $F(t)$ occurs at $t = t_{\max}$. Hence, $f(t_{\max}) = 0$, $f(t^-_{\max}) > 0$, and $f(t^+_{\max}) < 0$. We denote (25) as the *activation criterion* for (19). By the same argument, for the entire population to activate at some point, then we can derive the *entire activation criterion* as

$$F(t_{\max}) > \sigma(m_{crit}; \underline{m}_{\min}). \tag{26}$$

5.3 Numerical Simulation Issues and Derivation of an Averaged Nonautonomous Fisher's Equation

We depict the $u = 1$ isocline for a numerical simulation of (19) in Figure 2 with $g(m) = \alpha m(1-m)$, $f(t) = \beta \sin(\gamma t)$, $\alpha = 1/2, \beta = 1$, and $\gamma = 1.615$. These terms will be detailed more in Example 3 below. For numerical implementation, we use a standard central difference scheme for numerical integration along the x-dimension, an upwind scheme with flux limiters (similar to those described in [46]) to integrate along the m dimension, and a Crank-Nicholson scheme to integrate along time. From (25), we see that this simulation should not enter the active population with an initial condition of $\phi_1(m) = {}^{10}\!/_{3} I_{[.05,0.35]}(m)$, where $I_M(m)$ denotes an indicator function with support for $m \in M$. In Figure 2, however, we observe that the numerical simulation does enter the active population, which causes a significant portion of the population to incorrectly diffuse into the wound at a high rate.

Numerical simulations of advection-driven processes have been described as an "embarrassingly difficult" task, and one such problem is the presence of numerical diffusion [28, 46]. Numerical diffusion along the m-dimension is hard to avoid and here causes a portion of the cell population to enter the active population in situations where the it should approach the $m = m_{crit}$ plane but not pass it. Numerical diffusion can be reduced with a finer grid, but this can lead to excessively long computation times. With the aid of the activation curves given by (22), however, we can track progression of cells in the m-dimension analytically and avoid the problems caused by numerical diffusion completely.

To avoid the problems caused by numerical diffusion, we derive a nonautonomous Fisher's Equation for $w(t, x)$ that represents the average behavior along m with time-dependent diffusion and proliferation terms. To investigate the averaged cell population behavior along m over time, we integrate (19) over m to find

$$\begin{aligned} w_t(t,x) &= \left(D_1 w_{xx} + \lambda_1 w(1-w)\right) I_{[M_{inact}]}(m) \\ &\quad + \left(D_2 w_{xx} + \lambda_2 w(1-w)\right) I_{[M_{act}]}(m). \end{aligned} \tag{27}$$

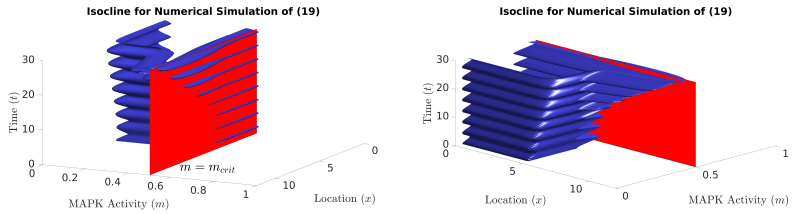

(a) (b)

Figure 2: Two views of the isocline for $u = 1$ from a numerical simulation of (19) with $g(m) = \alpha m(1-m)$ and $f(t) = \beta \sin(\gamma t)$ for $\alpha = 0.5, \beta = 1$, $\gamma = 1.615, D_1 = 0.01, D_2 = 1, \lambda_1 = 0.25$, and $\lambda_2 = 0.0025$ and an initial condition of $\phi_1(m) = {}^{10}/_{3} I_{[.05,0.35]}(m)$ and $\phi_2(x) = I_{[x \leq 5]}(x)$. The numerical scheme is discussed in Section 5.3 and the step sizes used are $\Delta m = {}^{1}/_{80}, \Delta x = {}^{1}/_{5}, \Delta t = 10^{-3}$. From (25), the simulation should not cross the $m = m_{crit}$ plane, which is given by the red plane. We see in frame (a) that the simulation does cross the $m = m_{crit}$ plane due to numerical diffusion, which causes the high rate of diffusion along x seen in frame (b).

An explicit form for (27) thus requires determining how much of the population is in the active and inactive populations over time. This is determined with the activation curves by calculating

$$\begin{aligned} h(t;\underline{m}) < m_{crit} \quad &\iff \quad F(t) < \sigma(m_{crit};\underline{m}) \\ &\iff \quad \underline{m} < \sigma^{-1}\left(-F(t); m_{crit}\right) =: \psi(t). \end{aligned} \tag{28}$$

Thus, $\underline{m} = \sigma^{-1}(-F(t); m)$ maps the distribution along m at time t back to the initial distribution, $\phi_1(\underline{m})$, and $\psi(t)$ denotes the threshold value in $\underline{m}$ between the active and inactive populations over time. $\Phi_1(\psi(t))$ thus denotes the portion of the population in the inactive population, and $1-\Phi_1(\psi(t))$ denotes the portion in the active population over time.

We thus derive a nonautonomous PDE for w, which we will term the *averaged nonautonomous Fisher's Equation*, as:

$$\begin{aligned} w_t &= D(t)w_{xx} + \lambda(t)w(1-w), \\ w(t=0,x) &= \phi_2(x) \\ w(t,x=-\infty) = 1 \qquad & w(t,x=\infty) = 0 \end{aligned} \tag{29}$$

where

$$\begin{aligned} D(t) &= D_2 + (D_1 - D_2)\Phi_1(\psi(t)) \\ \lambda(t) &= \lambda_2 + (\lambda_1 - \lambda_2)\Phi_1(\psi(t)). \end{aligned}$$

5.4 Three biologically-motivated examples

We next consider three examples of (19) that pertain to common patterns of biochemical activity during wound healing. We will use numerical simulations of (29) to investigate how different patterns of activation and deactivation over time affect the averaged cell population profile. We will also investigate how the profile changes when crossing the activation and entire activation thresholds derived in (25) and (26). In each example, we fix $m_{crit} = 0.5, D_1 = 0.01, D_2 = 1, \lambda_1 = .25,\ \lambda_2 = 0.0025, \phi_1(m) = {}^{10}/_{3} I_{[.05,0.25]}(m), \phi_2(x) = I_{(-\infty,5]}(x)$ and $g(m) = \alpha m(1-m)$, and use a different terms for $f(t)$ to mimic different biological situations. The choice for $g(m)$ ensures that the distribution along m stays between $m = 0$ and $m = 1$. A standard central difference scheme is used for numerical simulations of (29).

Example 1: Single Sustained MAPK activation wave: $f(t) = 1$

In this example, we consider a case where we observe the entire cell population approach a level of $m = 1$ over time. Such a scenario may represent the sustained wave of ERK 1/2 activity observed in MDCK cells from [31]. The authors of [41] proposed that the autocrine production of EGF caused this activation in the population. We use $f(t) = 1$ to observe this behavior.

Using (6) and (28), we find

$$\begin{aligned} \sigma(m;\underline{m}) &= \frac{1}{\alpha}\log\left(\frac{m}{1-m}\frac{1-\underline{m}}{\underline{m}}\right);\ \underline{m}, m \in (0,1) \\ h(t;\underline{m}) &= \sigma^{-1}(t;\underline{m}) = \underline{m}\left((1-\underline{m})e^{-\alpha t} + \underline{m}\right)^{-1} \\ \psi(t) &= (1+e^{\alpha t})^{-1} \end{aligned}$$

These functions demonstrate that the distribution along m is always activating along m but never reaches the $m = 1$ line, as $\sigma(m;\underline{m}) \to \infty$ as $m \to 1^-$ for any $\underline{m} \in (0,1)$. The entire population (excluding $\underline{m} = 0$) approaches $m = 1$ asymptotically, however, as $\lim_{t\to\infty} \sigma^{-1}(t;\underline{m}) = 1$. In Figure 3, we use (23) to depict the activation profile, $p(t,m)$, over time to show the activation behavior of the population. As expected, we observe the entire population converging to $m = 1$. We include some specific plots of the activation curves, $h(t;\underline{m})$, for this example. Note that the density changes along these curves by the height function $\frac{g(\sigma^{-1}(-F(t),m))}{g(m)}$, which is equivalent to the height function of the self-similar traveling wave ansatz made in (15).

In Figure 4(a), we depict a numerical simulation of $w(t,x)$ over time using (29). The slices denoted as "P" and "D" denote when the population is primarily proliferating ($\Phi_1(\psi(t)) > 1/2$) or diffusing ($\Phi_1(\psi(t)) \leq 1/2$) over time. The profile maintains a high cell density but limited migration into the wound during the proliferative phase and then migrates into the wound quickly during the diffusive phase but can not maintain a high cell density throughout the population. In Figure 4(b), we investigate how the profile of $w(t = 40, x)$ changes as α varies from $\alpha = 0$ to $\alpha = 0.2$. In the slice denoted "No activation", the

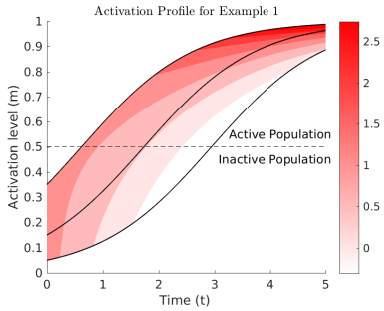

Figure 3: The analytical solution for the activation profile, $p(t, m)$, for Example 1 for $\alpha = 0.5$, and $\phi_1(m) = I_{(0.05,0.35)}(m)$. The solid black curves denote $h(t; \underline{m})$ for $\underline{m} = 0.05, 0.15$, and 0.35 and the dashed line denotes $m = m_{crit}$. Note that a log scale is used along p for visual ease.

entire population is still in the inactive population at $t = 40$ and thus does not progress far into the wound or change with α. In the slice denoted "Activation," the population is split between the active and inactive populations at $t = 40$. The profiles here are sensitive to increasing values of α, as they migrate further into the wound while maintaining a high density near $x = 0$. The slice denoted as "Entire Activation" denotes simulations that are entirely in the active population by $t = 40$. As α increases, these simulations do not migrate much further into the wound but do have decreasing densities at $x = 0$. These results suggest that a combination of proliferation and diffusion must be used to maximize population migration while maintaining a high cellular density behind the population front. The optimal combination appears to occur at the entire activation threshold.

Example 2: Single pulse of MAPK activation: $f(t) = \beta e^{\gamma t} - 1$

We now detail an example that exhibits a pulse of activation in the m dimension, which may represent the transient wave of ERK 1/2 activation observed in MDCK cells in [31]. The authors of [41] proposed that this wave may be caused by the rapid production of ROS in response to the wound, followed by the quick decay of ROS or its consumption by cells. We now let $f(t) = \beta e^{\gamma t} - 1$. This forcing function arises if ROS is present but decaying exponentially over time and modeled by $s(t) = \beta e^{\gamma t}, \beta > 0, \gamma < 0$ and cells activate linearly in response to the presence of ROS but have a baseline level of deactivation, which may be given by $f(s) = s - 1$.

We see that $\sigma(m; \underline{m})$ and $\sigma^{-1}(t; \underline{m})$ are the same as in Example 1 and now

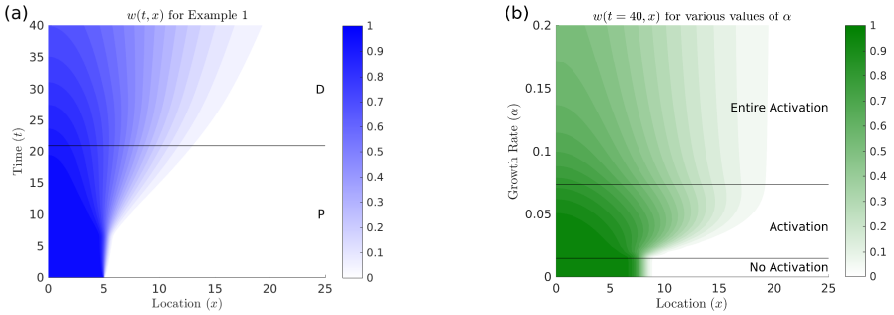

Figure 4: Numerical simulations of the averaged nonautonomous Fisher's equation for Example 1. In (a), we depict a simulation of $w(t,x)$ over time for $\alpha = 0.05$. The letters "P" and "D" denote when the population is primarily proliferating or diffusing, respectively. In (b), we depict how the profile for $w(t=40,x)$ changes for various values of α. The descriptions "No Activation", "Activation", and "Entire Activation" denote values of α for which the population is entirely in the inactive population, split between the active and inactive populations, or entirely in the active population at $t = 40$, respectively.

compute

$$\begin{aligned} h(t;\underline{m}) &= \underline{m}\left(\underline{m} + (1-\underline{m})\exp\left[\alpha t - \frac{\alpha\beta}{\gamma}(\exp(\gamma t)-1)\right]\right)^{-1} \\ \psi(t) &= \left(1+\exp\left[-\alpha t + \frac{\alpha\beta}{\gamma}(\exp(\gamma t)-1)\right]\right)^{-1}. \end{aligned}$$

In Figure 5, we use (23) to depict the activation profile, $p(t,m)$, over time to show the activation behavior of the population. We also include some specific plots of the activation curves, $h(t;\underline{m})$, which show a pulse of MAPK activity in the population that starts decreasing around $t = 5$. Note that $h(t;0.35)$ crosses the $m = m_{crit}$ line but $h(t;0.05)$ does not, so (25) is satisfied for this parameter set (the population becomes activated) but (26) is not (the entire population does not become activated).

Using (25), we determine our activation criterion for this example as

$$\frac{1-\beta+\log\beta}{\gamma} > \frac{1}{\alpha}\log\left(\frac{m_{crit}}{1-m_{crit}}\frac{1-\underline{m}_{\max}}{\underline{m}_{\max}}\right).$$

If we fix $\gamma = -1, \alpha = 1, m_{crit} = 0.5, \underline{m}_{\max} = 0.35$, and $\underline{m}_{\min} = 0.05$, we find that the above inequality is satisfied for β approximately greater than 2.55. This may represent a scenario in which we know the decay rate of the ROS through γ, the activation rate of the MAPK signaling cascade through α, the MAPK activation distribution before ROS release with $\underline{m}_{\min}$ and $\underline{m}_{max}$, and the activation threshold with m_{crit}. The values of β denote the concentration of released ROS, which should be at least 2.55 to see the population activate. We similarly find that the entire population will activate at some time for $\beta > 5.68$.

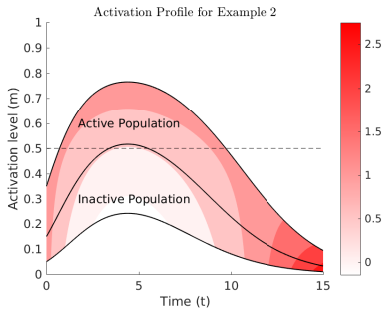

Figure 5: The analytical solution for the activation profile, $p(t, m)$, for Example 2 for $\alpha = 0.5, \beta = 3, \gamma = -1/4$ and $\phi_1(m) = I_{(0.05,0.35)}(m)$. The solid black curves denote $h(t; \underline{m})$ for $\underline{m} = 0.05, 0.15$, and 0.35 and the dashed line denotes $m = m_{crit}$. Note that a log scale is used along p for visual ease.

In Figure 6(a), we depict a numerical simulation of (29) for this example. The population quickly transitions to a diffusing stage due to the pulse of MAPK activation and shows the smaller densities (u approximately less than 0.2) migrating into the wound rapidly while the density behind the population front drops. As the pulse of MAPK activation ends and the population transitions back to a proliferating phenotype, the populations restores a high density behind the cell front and begins to develop a traveling wave profile, as suggested by the parallel contour lines. In Figure 6(b), we investigate how the profile for $w(t = 30, x)$ changes as β varies from $\beta = 2$ to $\beta = 9$ while keeping all other parameters fixed. We observe that the profile is the same for all values of $\beta < 2.55$, as (25) is not satisfied. As β increases past the activation threshold, the profile shows increased rates of migration into the wound. After passing the entire activation threshold (26), the profile continues to migrate further as β increases, but appears less sensitive to β. This increased migration is likely due to the population spending more time in the active population for larger values of β. Note that for all simulations shown, the pulse of MAPK activation has finished by $t = 30$.

Example 3: Periodic pulses of MAPK activation: $f(t) = \beta \sin(\gamma t)$

As a last example, we exhibit a scenario with periodic waves of activity. Such behavior was observed in some of the experiments performed in [51], in which cell cultures of the HaCaT cell line were periodically treated with TGF-β to investigate how periodic treatment with TGF-β affects activation of the SMAD pathway (the canonical pathway for TGF-β, which also influences cell proliferation and migration). We let $f(t) = \beta \sin(\gamma t), \beta, \gamma > 0$, which occurs if the concentration of TGF-β over time is given by $s(t) = 1 + \sin(\gamma t)$, and cells activate linearly in response to s and have a baseline rate of deactivation, given by $f(s) = \beta(s - 1)$.

We now calculate

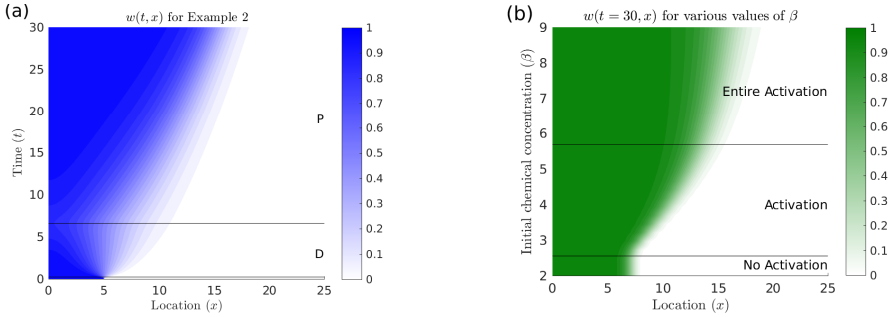

Figure 6: Numerical simulations of the averaged nonautonomous Fisher's equation for Example 2. In (a), we depict a simulation of $w(t,x)$ over time for $\alpha = 1, \beta = 8, \gamma = -1$. Slices denoted with a "P" or "D" denote when the population is primarily proliferating or diffusing, respectively. In (b), we depict how the profile for $w(t = 30, x)$ changes for various values of β. The descriptions "No activation", "Activation", and "Entire Activation" denote values of β for which the population is entirely in the inactive population, split between the active and inactive populations, or entirely in the active population at $t = t_{\max}$.

$$h(t;\underline{m}) = \underline{m}\left(\underline{m} + (1-\underline{m})\exp\left[\frac{\alpha\beta}{\gamma}\left(\cos(\gamma t) - 1\right)\right]\right)^{-1}$$

$$\psi(t) = \left(1 + \exp\left[\frac{\alpha\beta}{\gamma}(1-\cos(\gamma t))\right]\right)^{-1}.$$

In Figure 7, we use (23) to depict the activation profile, $p(t,m)$, over time to show the activation behavior of the population. We also include some specific plots of the activation curves $h(t;\underline{m})$, which demonstrate periodic waves of activation along m. Note that $h(t;0.05)$ crosses the $m = m_{crit}$ line, so (26) is satisfied, and the entire population becomes activated at some points during the simulation.

The activation criterion (25) can be solved as

$$\frac{2\beta}{\gamma} > \frac{1}{\alpha}\log\left(\frac{m_{crit}}{1-m_{crit}}\frac{1-\underline{m}_{\max}}{\underline{m}_{\max}}\right).$$

We thus calculate that if we fix $\beta = 1, \alpha = 1/2, \underline{m}_{max} = 0.35, \underline{m}_{\min} = 0.05$, and $m_{crit} = 0.5$, then the activation criterion (25) is satisfied for $\gamma < 1.615$ and the entire activation criterion (26) is satisfied for $\gamma < 0.34$. These estimates would tell us how frequently signaling factor treatment is needed to see different patterns of activation in the population.

In Figure 8(a), we depict a numerical simulation of (29) for this example. The population phenotype has a period of 4π, and we see that the lower densities migrate into the wound most during the diffusive stages, whereas all densities appear to migrate into the wound at similar speeds during the proliferative

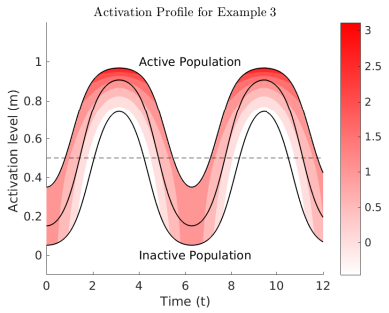

Figure 7: The analytical solution for the activation profile, $p(t, m)$, for Example 3 for $\alpha = 1/2, \beta = 4, \gamma = 1$ and $\phi_1(m) = I_{(0.05,0.35)}(m)$. The solid black curves denote $h(t; \underline{m})$ for $\underline{m} = 0.05, 0.15$, and 0.35 and the dashed line denotes $m = m_{crit}$. Note that a log scale is used along p for visual ease.

stages. In Figure 8(b), we investigate how the profile for $w(t = 40, x)$ changes as γ varies between $\gamma = 0$ and $\gamma = 1.9$ while keeping all other parameters fixed. All profiles appear the same for $\gamma > 1.615$ as (25) is not satisfied. As γ decreases below this threshold, more of the population becomes activated during the simulation, culminating in a maximum propagation of the population at the entire activation threshold, $\gamma \approx 0.34$. As γ falls below γ=0.34, the population tends to migrate less, although the population does migrate far for γ near 0.2. For $\gamma < 0.2$, the population appears to spend too much time in the active population and diffuses excessively with limited proliferation. These simulations lead to shallow profiles that do not migrate far into the wound. As γ approaches zero, the simulations would become entirely activated, but do not before $t = 40$. These simulations stay in the inactive population for the duration of the simulation and do not migrate far into the wound.

6 Discussion and Future work

We have investigated a structured Fisher's Equation that incorporates an added dimension for biochemical activity that influences population migration and proliferation. The method of characteristics proved to be a useful way to track the progression along the population activity dimension over time. With the aid of a phase plane analysis and an asymptotically autonomous Poincare-Bendixson Theorem, we were able to prove the existence of a self-similar traveling wave solution to the equation when diffusion and proliferation do not depend on MAPK activity. The height function of the self-similar traveling wave ansatz along characteristic curves is demonstrated in Figures 3, 5, and 7. We believe our analysis could be extended to investigate structured versions of other nonlinear PDEs.

Activation of the MAPK signaling cascade is known to influence collective migration during woung healing through cellular migration and proliferation

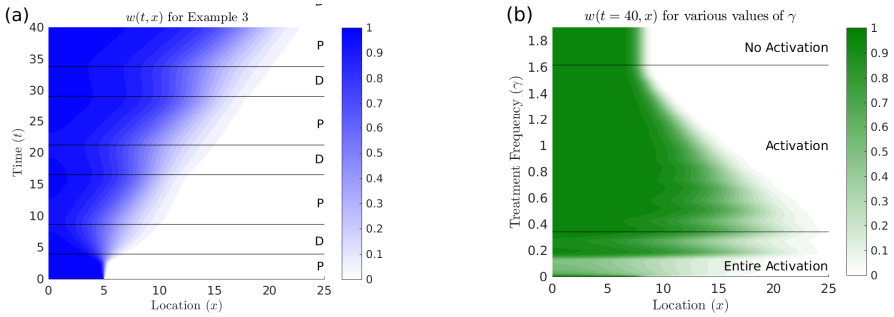

Figure 8: Numerical simulations of the averaged nonautonomous Fisher's equation for Example 3. In (a), we depict a simulation of $w(t,x)$ over time for $\alpha = 0.5, \beta = 1$, and
$\gamma = 1/2$. Slices denoted with a "P" or "D" denote when the population is primarily proliferating or diffusing, respectively. In (b), we depict $w(t = 40, x)$ for various values of γ. The descriptions "No activation", "Activation", and "Entire Activation" denote values of γ for which the population is entirely in the inactive population, split between the active and inactive populations, or entirely in the active population at $t = t_{\max}$.

properties. For this reason, we also considered a structured PDE model in which the rates of cellular diffusion and proliferation depend on the levels of MAPK activation in the population. We also extended the model to allow for the presence of an external cytokine or growth factor that regulates activation and deactivation along the MAPK signaling cascade. We derived two activation criteria for the model to establish conditions under which the population will become activated during simulations. As numerical simulations of the structured equation are prone to error via numerical diffusion, we derived a nonautonomous equation in time and space to represent the average population behavior along the biochemical activity dimension. Using this nonautonomous equation, we exhibited three simple examples that demonstrate biologically relevant activation levels and their effects on population migration: a sustained wave of activity, a pulse of activity, and periodic pulses of activity. We found that the population tends to migrate farthest while maintaining a high cell density at the entire activation threshold value, (26), for the sustained wave and periodic pulse patterns of activation. The single pulse case continued migrating further into the wound after passing the entire activation threshold but appeared less sensitive after doing so.

A natural next step for this analysis is to use a structured population model of this sort in combination with biological data to thoroughly investigate the effects of MAPK activation and deactivation on cell migration and proliferation during wound healing. Previous mathematical models have focused on either collective migration during wound healing assays in response to EGF treatment (while neglecting the MAPK signaling cascade) [21, 37] or MAPK propagation

during wound healing assays (while neglecting cell migration) [41]. To the best of our knowledge, no mathematical models have been able to reliably couple signal propagation and its effect on cell migration during wound healing. The examples detailed in this work intentionally used the simplest terms possible as a means to focus on the underlying mathematical aspects. With a separate in-depth study into the biochemistry underlying the MAPK signaling cascade and its relation with various cytokines or growth factors, more complicated and biologically relevant terms for $g(m), f(s)$, and $s(t)$ can be determined to help elucidate the effects of MAPK activation on cell migration during wound healing.

The analytical techniques used in this study cannot be used to investigate spatial patterns of biochemical activity due to the parabolic nature of (3) in space. Cell populations also migrate via chemotaxis during wound healing, in which cells migrate up a concentration gradient of some chemical stimulus [2, 23, 26, 38]. Chemotactic equations are hyperbolic in space, which may facilitate spatial patterns of MAPK activation during wound healing, such as those described experimentally in [7]. As various pathways become activated and cross-talk during wound healing to influence migration [16], future studies could also investigate a population structured along multiple signaling pathways, $u(t, x, \vec{m})$ for the vector $\vec{m} = (m_1, m_2, \ldots, m_n)^T$. Because the cell population also produces cytokines and growth factors for paracrine and autocrine signaling during wound healing, these models would also benefit from unknown variables representing ROS, TGF-β, EGF, etc.

While the main motivation for this study is epidermal wound healing, there are potential applications in other areas of biology. Fisher's equation has also been used to study population dynamics in ecology and epidemiology [1, 19, 44]. Our framework could be extended to a case where an environmental effect, such as seasonal forcing, impacts species migration or susceptibility of individuals to disease. The results presented here may thus aid in a plethora of mathematical biology studies.

References

[1] S. Ai and W. Huang, *Travelling waves for a reaction-diffusion system in population dynamics and epidemiology*, Proceedings of the Royal Society of Edinburgh Section A: Mathematics, 135 (2005), pp. 663–675.

[2] S. Ai, W. Huant, and Z.-a. Wang, *Reaction, Diffusion and chemotaxis in wave propagation*, Discrete and Continuous Dynamical System - B, 20 (2015), pp. 1–21.

[3] H. T. Banks and H. T. Tran, *Mathematical and Experimental Modeling of Physical and Biological Processes*, CRC Press, Boca Raton, FL, 2009.

[4] S. P. Blythe, K. Cooke, and C. Castillo-Chavez, *Autonomous Risk-behavior change, and non-linear incidence rate, in models of sexually transmitted diseases*, (1991).

[5] A. Q. Cai, K. A. Landman, and B. D. Hughes, *Multi-scale modeling of a wound-healing cell migration assay*, Journal of Theoretical Biology, 245 (2007), pp. 576–594.

[6] C. Castillo-Chavez and H. R. Thieme, *Asymptotically Autonomous Epidemic Models*, (1994).

[7] D. A. Chapnick and X. Liu, *Leader cell positioning drives wound-directed collective migration in TGF beta-stimulated epithelial sheets*, Mol. Biol. Cell, 25 (2014), pp. 1586–1593.

[8] R. A. F. Clark and P. Henson, *The Molecular and Cellular Biology of Wound Repair*, Plenum Press, New York, second ed., 1995.

[9] C. W. Curtis and D. M. Bortz, *Propagation of fronts in the Fisher-Kolmogorov equation with spatially varying diffusion*, Physical Review E, 86 (2012).

[10] A. M. de Roos, *A gentle introduction to physiologically structured population models*, in Structured-Population Models in Marine, Terrestrial, and Freshwater Systems, Population and Community Biology Series, 1996.

[11] P. K. Denman, D. L. S. McElwain, and J. Norbury, *Analysis of Travelling Waves Associated with the Modelling of Aerosolised Skin Grafts*, Bull. Math. Biol., 69 (2006), pp. 495–523.

[12] A. Ducrot, *Travelling waves for a size and space structured model in population dynamics: Point to sustained oscillating solution connections*, Journal of Differential Equations, 250 (2011), pp. 410–449.

[13] A. Ducrot, P. Magal, and S. Ruan, *Travelling Wave Solutions in Multigroup Age-Structured Epidemic Models*, Arch Rational Mech Anal, 195 (2009), pp. 311–331.

[14] R. A. Fisher, *The wave of advance of advantageous genes*, Annals of Eugenics, 7 (1937), pp. 353–369.

[15] S. Gourley, R. Liu, and J. Wu, *Some Vector Borne Diseases with Structured Host Populations: Extinction and Spatial Spread*, SIAM J. Appl. Math., 67 (2007), pp. 408–433.

[16] X. Guo and X.-F. Wang, *Signaling cross-talk between TGF-beta/BMP and other pathways*, Cell Res, 19 (2009), pp. 71–88.

[17] M. E. Gurtin and R. C. Maccamy, *Non-linear age-dependent population dynamics*, Arch. Rational Mech. Anal., 54 (1974), pp. 281–300.

[18] J. F. Hammond and D. M. Bortz, *Analytical solutions to Fisher's equation with time-variable coefficients*, Applied Mathematics and Computation, 218 (2011), pp. 2497–2508.

[19] A. Hastings, K. Cuddington, K. F. Davies, C. J. Dugaw, S. Elmendorf, A. Freestone, S. Harrison, M. Holland, J. Lambrinos, U. Malvadkar, B. A. Melbourne, K. Moore, C. Taylor, and D. Thomson, *The spatial spread of invasions: new developments in theory and evidence*, Ecology Letters, 8 (2005), pp. 91–101.

[20] W. Jin, E. T. Shah, C. J. Penington, S. W. McCue, L. K. Chopin, and M. J. Simpson, *Reproducibility of scratch assays is affected by the initial degree of confluence: Experiments, modelling and model selection*, Journal of Theoretical Biology, 390 (2016), pp. 136–145.

[21] S. T. Johnston, E. T. Shah, L. K. Chopin, D. L. Sean McElwain, and M. J. Simpson, *Estimating cell diffusivity and cell proliferation rate by interpreting IncuCyte ZOOM assay data using the Fisher-Kolmogorov model*, BMC Systems Biology, 9 (2015).

[22] J. P. Keener and J. Sneyd, *Mathematical Physiology: I Cellular Physiology*, vol. 8/I of Interdisciplinary Applied Mathematics, Springer, second ed., 2009.

[23] E. F. Keller and L. A. Segel, *Traveling bands of chemotactic bacteria: a theoretical analysis*, Journal of Theoretical Biology, 30 (1971), pp. 235–248.

[24] A. Kolmogoroff, I. Petrovsky, and N. Piscounoff, *Etude de l'equation de la diffusion avec croissance de la quantite de matiere et son application a un probleme biologique*, Moscow Univ. Bull. Math, 1 (1937), pp. 1–25.

[25] Y. Kuang, E. M. Rutter, and T. L. Stepien, *A data-motivated density-dependent diffusion model of in vitro glioblastoma growth*, Mathematical Biosciences and Engineering, 12 (2015), pp. 1157–1172.

[26] K. Landman, M. Simpson, J. Slater, and D. Newgreen, *Diffusive and Chemotactic Cellular Migration: Smooth and Discontinuous Traveling Wave Solutions*, SIAM J. Appl. Math., 65 (2005), pp. 1420–1442.

[27] K. A. Landman, A. Q. Cai, and B. D. Hughes, *Travelling Waves of Attached and Detached Cells in a Wound-Healing Cell Migration Assay*, Bull. Math. Biol., 69 (2007), pp. 2119–2138.

[28] B. P. Leonard, *The ULTIMATE conservative difference scheme applied to unsteady one-dimensional advection*, Computer Methods in Applied Mechanics and Engineering, 88 (1991), pp. 17–74.

[29] P. K. Maini, D. S. McElwain, and D. I. Leavesley, *Traveling wave model to interpret a wound-healing cell migration assay for human peritoneal mesothelial cells*, Tissue engineering, 10 (2004), pp. 475–482.

[30] L. Markus, *Asymptotically autonomous differential systems*, in Contributions to the theory of nonlinear oscillations, vol. III of Annals of Mathematics Studies, Princeton University Press, 1956.

[31] Y. Matsubayashi, M. Ebisuya, S. Honjoh, and E. Nishida, *ERK Activation Propagates in Epithelial Cell Sheets and Regulates Their Migration during Wound Healing*, Current Biology, 14 (2004), pp. 731–735.

[32] A. G. McKendrick, *Applications of mathematics to medical problems*, 1927.

[33] J. D. Meiss, *Differential Dynamical Systems*, SIAM, 2007.

[34] J. D. Murray, *Lectures on nonlinear-differential equation models in biology*, Oxford University Press, 1977.

[35] J. D. Murray, *Mathematical Biology I. An Introduction*, vol. 17 of Interdisciplinary Applied Mathematics, Springer New York, New York, NY, 3rd ed., 2002.

[36] P. J. Murray, J.-W. Kang, G. R. Mirams, S.-Y. Shin, H. M. Byrne, P. K. Maini, and K.-H. Cho, *Modelling Spatially Regulated beta-Catenin Dynamics and Invasion in intestinal Crypts*, Biophysical Journal, 99 (2010), pp. 716–725.

[37] J. T. Nardini, D. A. Chapnick, X. Liu, and D. M. Bortz, *Modeling keratinocyte wound healing: cell-cell adhesions promote sustained migration*, Journal of Theoretical Biology, 400 (2016), pp. 103–117.

[38] D. Newgreen, G. Pettet, and K. Landman, *Chemotactic Cellular Migration: Smooth and Discontinuous Travelling Wave Solutions*, SIAM J. Appl. Math., 63 (2003), pp. 1666–1681.

[39] A. Perumpanani, B. Marchant, and J. Norbury, *Traveling Shock Waves Arising in a Model of Malignant Invasion*, SIAM J. Appl. Math., 60 (2000), pp. 463–476.

[40] G. J. Pettet, H. M. Byrne, D. L. S. Mcelwain, and J. Norbury, *A model of wound-healing angiogenesis in soft tissue*, Mathematical Biosciences, 136 (1996), pp. 35–63.

[41] F. Posta and T. Chou, *A mathematical model of intercellular signaling during epithelial wound healing*, Journal of Theoretical Biology, 266 (2010), pp. 70–78.

[42] F. R. Sharpe and A. J. Lotka, *A problem in Age-Distribution*, Philosphical Magazine, 21 (1911), pp. 435–438.

[43] J. A. Sherratt and M. A. J. Chaplain, *A new mathematical model for avascular tumour growth*, J Math Biol, 43 (2001), pp. 291–312.

[44] N. Shigesada and K. Kawasaki, *Biological Invasions: Theory and Practice*, Oxford Series in Ecology and Evolution, Oxford University Press, 1997.

[45] J. W.-H. So, J. Wu, and X. Zou, *A reaction-diffusion model for a single species with age structure. I Travelling wavefronts on unbounded domains*, Proceedings of the Royal Society of London A: Mathematical, Physical and Engineering Sciences, 457 (2001), pp. 1841–1853.

[46] J. A. Thackham, D. L. S. McElwain, and I. W. Turner, *Computational Approaches to Solving Equations Arising from Wound Healing*, Bull. Math. Biol., 71 (2008), pp. 211–246.

[47] H. R. Thieme, *Convergence results and a Poincare-Bendixson trichotomy for asymptotically autonomous differential equations*, J. Math. Biol., 30 (1992), pp. 755–763.

[48] H. R. Thieme, *Asymptotically Autonomous Differential Equations in the Plane*, Rocky Mountain J. Math., 24 (1993), pp. 351–380.

[49] A. Volpert, V. Volpert, and V. Volpert, *Traveling Wave Solutions of Parabolic Systems*, vol. 140 of Translations of Mathematical Monographs, American Mathematical Society, 1994.

[50] G. F. Webb, *Population models structured by age, size, and spatial position*, in Structured Population Models in Biology and Epidemiology, Springer, 2008, pp. 1–49.

[51] Z. Zi, Z. Feng, D. A. Chapnick, M. Dahl, D. Deng, E. Klipp, A. Moustakas, and X. Liu, *Quantitative analysis of transient and sustained transforming growth factor-beta signaling dynamics*, Molecular Systems Biology, 7 (2011), p. 492.

A Properties of $\sigma^{-1}(t;\underline{y})$

If we assume that g is positive and uniformly continuous, then $\sigma^{-1}(t;\underline{y})$ exists and satisfies the following:

$$\frac{d}{dt}\sigma^{-1}(t;\underline{y}) = g(\sigma^{-1}(t;\underline{y})),\ \sigma^{-1}(0;\underline{y}) = \underline{y}. \tag{30}$$

To derive (30), see that

$$\begin{aligned} y(t) &= \sigma^{-1}(t;\underline{y}) \\ \Rightarrow \sigma(y(t);\underline{y}) &= t \\ \Rightarrow \frac{d}{dt}\left(\sigma(y(t);\underline{y})\right) = \frac{d}{dy}\sigma(y(t);s)\frac{dy}{dt} &= 1 \\ \Rightarrow \frac{1}{g(y(t))}\frac{dy}{dt} &= 1 \\ \Rightarrow \frac{dy}{dt} &= g(y(t)) \\ \Rightarrow \frac{d}{dt}\sigma^{-1}(t;\underline{y}) &= g(\sigma^{-1}(t;y)). \end{aligned}$$

and for the initial condition,

$$\begin{aligned} \sigma(\underline{y},\underline{y}) &= 0 \\ \Rightarrow \sigma^{-1}(0,\underline{y}) &= \underline{y}. \end{aligned}$$

B Derivation of (9)

In (8), we defined

$$v(t;\underline{y}) := u(t, y = \sigma^{-1}(t;\underline{y})).$$

Taking the derivative of $v(t;\underline{y})$ with respect to time, we find with the aid of the chain rule:

$$\begin{aligned} \frac{d}{dt}v(t;\underline{y}) &= \frac{\partial}{\partial t}u(t, y = \sigma^{-1}(t;\underline{y})) + \frac{\partial}{\partial y}u(t, y = \sigma^{-1}(t;\underline{y})) \cdot \frac{d}{dt}\sigma^{-1}(t;\underline{y}) \\ &= -\frac{\partial}{\partial y}\left[g\left(\sigma^{-1}(t;\underline{y})\right) u\left(t, y = \sigma^{-1}(t;\underline{y})\right)\right] \\ &\quad + Au\left(t, y = \sigma^{-1}(t;\underline{y})\right) + g\left(\sigma^{-1}(t;\underline{y})\right)\frac{\partial}{\partial y}u\left(t, y = \sigma^{-1}(t;\underline{y})\right) \\ &= -g'(\sigma^{-1}(t;\underline{y}))v(t;\underline{y}) + Av(t;\underline{y}). \end{aligned}$$

C Relevant Material on Asymptotically Autonomous Differential Systems

The theorem statements in this section have been slightly modified to match notation from our study. Consider the two vector fields,

$$\dot{x} = f(t,x) \tag{31}$$

$$\dot{y} = g(y), \tag{32}$$

for $x, y \in \mathbb{R}^n$ and $t > 0$. Assume $f(t,x)$ and $g(x)$ are continuous in t and x and locally Lipschitz in x for $x \in \Omega$ and $t > 0$, where Ω is an open subset of

$\mathbb{R}^n$. We say that (31) is asymptotically autonomous with limit equation (32) if $f(t,x) \to g(x)$ pointwise as $t \to \infty$ on any compact subset of Ω.

We will denote the ω-limit sets for all points starting in the set $\Theta \subset \Omega$ at $t = 0$ for the system (31) as $\omega_f(\Theta)$. This asymptotically autonomous Poincare-Bendixson Theorem was introduced in [30] and states

Asymptotically Autonomous Poincare-Bendixson Theorem:

Let $n = 2$ and (31) be asymptotically autonomous with limit equation (32) in $\Omega \subset \mathbb{R}^2$. Let a solution, $x(t)$, of (31) lie in a compact set $\Theta \subset \Omega$ for large t and suppose $\omega_f(\Theta)$ contains no equilibria of (32). Then $\omega_f(\Theta)$ is the union of periodic orbits of (32).

The proof of this Theorem is a result of the standard Poincare-Bendixson Theorem (see [33, Section 6.6]) and the following theorem, which is also proved in [30].

Theorem: Let (31) be asymptotically autonomous with limit equation (32) in $\Omega \in \mathbb{R}^n$. Let P be a stable equilibrium point of (32). Then there is a neighborhood, N, of P and a time T such that $\omega_f(N) = \{P\}$ for all solutions of (31) starting at time T or later.